MICROSTRUCTURE AND TENSILE PROPERTIES OF AL PM PREPARED BY NOVEL LOW-PRESSURE SINTERING

Results from a study showed it was difficult for pressureless sintering to densify pre-alloyed aluminum powders, but low-pressure sintering could.

By LEI WU, ZHAOJI YU, CHAO LIU, YUNZHU MA, YUFENG HUANG, TAO WANG, LUN YANG, HUANYUAN YAN, and WENSHENG LIU

This article proposes a novel low-pressure sintering process contraposing to characteristics of pre-alloyed aluminum powders and analyzes its feasibility. The low pressure was set to 0.1 MPa in this study. Meanwhile, 0 MPa and 10 MPa were set as the control group. With gas-atomized 2024 aluminum powders as raw material, the microstructure and tensile properties of specimens sintered under three orders of magnitude of pressure (0 MPa, 0.1 MPa, and 10 MPa) at two representative temperatures (525°C and 575°C) were compared. The results showed it was difficult for pressureless sintering (0 MPa) to densify pre-alloyed aluminum powders, but low-pressure sintering could. As the liquid phase formed at supersolidus temperature was squeezed out, the loss of alloying elements such as Cu and Mg, which would play an important role in subsequent heat treatment, during low-pressure sintering was apparently less than that of 10 MPa. The density of aluminum sintered under 0.1 MPa at 575°C was 2.732 g/cm^3 and the ultimate tensile strength was 228.16 MPa with ductility of 12%, which achieved a good balance of plasticity and strength. These findings will bring new insights to the industrialization of aluminum powder metallurgy (APM).

1 INTRODUCTION

Aluminum and its alloys are the most often used light metal due to their attractive properties [1]. Tapping the application potential of aluminum alloy has always been the focus because of exuberant demands in the field of aerospace and vehicle manufacturing. As an advanced manufacturing technology of aluminum alloys, powder metallurgy has unique characteristics: flexible composition design, special material structurally different from cast metal, and cost advantage of near net forming. Based on these, aluminum powder metallurgy (APM) technology is very suitable for manufacturing aluminum-based composite materials and gradient materials. Rahimian et al. [2] studied the effect of temperature, time, and particle size on the preparation of Al–Al_2O_3 by powder metallurgy. Sun et al. [3] employed powder metallurgy to prepare SiC-reinforced pure aluminum composites. A Graphene oxide-reinforced aluminum composite was fabricated by powder metallurgy [4]. Apparently, APM will be a breakthrough for traditional aluminum alloy industry.

Despite owning unique performances, the industrialized development of APM is seriously delayed due to the current unsatisfactory APM technology [5]. The mainstream APM process is divided into liquid phase sintering with element-mixed powders as a raw material [5] and hot pressing with pre-alloyed powders. Although the liquid phase sintering is simple and economical, the inferior mechanical properties of sintered components are usually unable to serve for industrial products, which rely heavily on subsequent machining. Boland et al. [6] mentioned the commercial APM was limited due to the correspondingly narrow scope of mechanical properties. Sweet et al. [7] used powder forge to improve mechanical properties of APM.

As another choice for APM, the components fabricated by hot pressing with the microstructure and mechanical properties similar to those of cast aluminum have near full density and good mechanical properties. However, the inescapable problem is the current hot pressing process for APM always requires high loading pressure (>10 MPa) to ensure high density. Cooke et al. [8] sintered Al powder with 0.4% Sc using spark plasma sintering (SPS) under 50 MPa at 550°C. The relative density of the corresponding aluminum was more than 99.5% and the tensile strength was 226 MPa; Khalil et al. [9] optimized the SPS process for 6061 aluminum and 2124 aluminum and confirmed the best process parameter was 450°C and 35 MPa; Wang et al. [10] adopted hot isostatic pressing (HIP) at 580°C under 130 MPa for 3 hours to obtain the sintered aluminum alloy with a density of 98.9% and tensile strength of 324 MPa.

All of the above cases about hot pressing of aluminum powders rely on complex and expensive sintering equipment, but their low production efficiency is unqualified to satisfy modern industrial production demands. It completely offset the cost advantage of powder metallurgy as a near-net forming technology, leading to the current APM unable to form a significant advantage for the traditional aluminum industry. Actually, for some aluminum base components with simple shapes and small sizes, there is no need for high loading pressure. In other words, the complex hydraulic system could be replaced by the gravity of heavy weight, a kind of low-pressure state, which may be suitable for automatic production in a mesh belt furnace. This approach will greatly improve the production efficiency of APM and significantly reduce production cost. However, to date, there have been few studies on the sintering of aluminum powder under low pressure.

The purpose of this research is a feasibility analysis of low-pressure sintering for aluminum powders in an effort to open up a new field for APM industry. In this work, pressureless sintering (0 MPa) and pressure sintering with 10 MPa were set as control group. The reason for choosing 10 MPa is it is of the same order of magnitude as the pressure used in mainstream hot pressing for APM. Meanwhile, the low pressure was set to 0.1 MPa, which was two orders of magnitude lower than 10 MPa and easily achieved by a heavy weight. The microstructure and tensile properties of aluminum alloys sintered under three different magnitudes of pressure (0 MPa, 0.1 MPa, and 10 MPa) were systematically compared to evaluate low-pressure sintering for APM.

2 EXPERIMENTAL

2.1 Raw materials

In this work, 2024Al nitrogen atomized powders produced by Changsha Tianjiu Co. were used as the raw material, and the chemical composition is listed in Table 1. Figure 1 exhibits the morphology, cross-sectional microstructure, differential scanning calorimetry

(DSC) curve, and particle size distribution of as-received powders. The atomized powders were nearly spherical, and some of them cohered with each other during the solidification of molten droplets (Figure 1a). As indicated in Figure 1b, the cross-section microstructure consisted of dendrite crystals and cellular crystals, which is a typical rapid solidification feature. According to the results of an energy dispersive spectrometer (EDS) in the dendrite crystal (A point) and at the dendrite boundary (B point), the alloying elements of Cu and Mg in the powder were mainly enriched in the dendrite boundary. Figure 1c presents the DSC curve of 2024Al powders analyzed by a NETZSCH STA 449F3 integrated thermal analyzer. It can be seen that a small endothermic peak appears at 507°C, and the temperature corresponding to the peak value of the main endothermic peak, which also is the melt point of this pre-alloyed powder, is 648°C. The small endothermic peak appearing at 507°C indicated there was a phase transition during heating. According to the phase diagram [7], the phase transition actually corresponds to the eutectic reaction, which leads to the formation of a liquid phase in the aluminum. Thus, the solidus of as-received powders was 507°C. Figure 1d shows the particle size distribution of powder particles that the average particle size Dv50 was 68.7 μm.

Element	Cu	Mg	Zn	Fe	Si	Mn	Al
2024Al	4.07	1.51	0.33	0.14	0.094	0.071	Bal

Table 1: Chemical composition of 2024 pre-alloy powder (wt%).

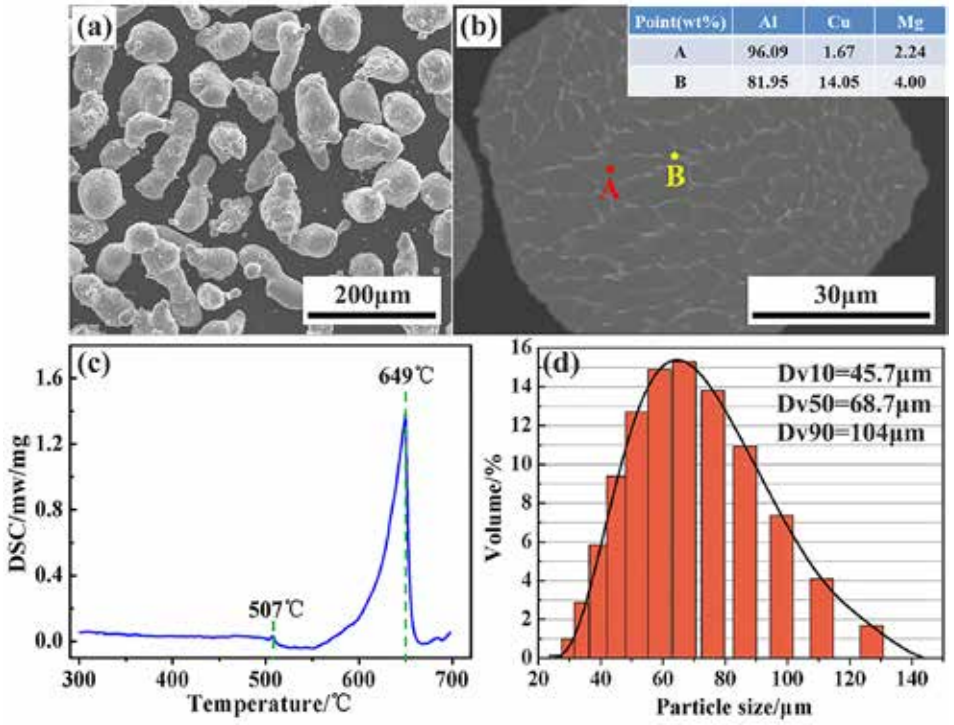

Figure 1: Powder characteristics of 2024 atomized powders: (a) morphology, (b) cross-sectional microstructure (wt%), (c) DSC curve, (d) particle size distribution.

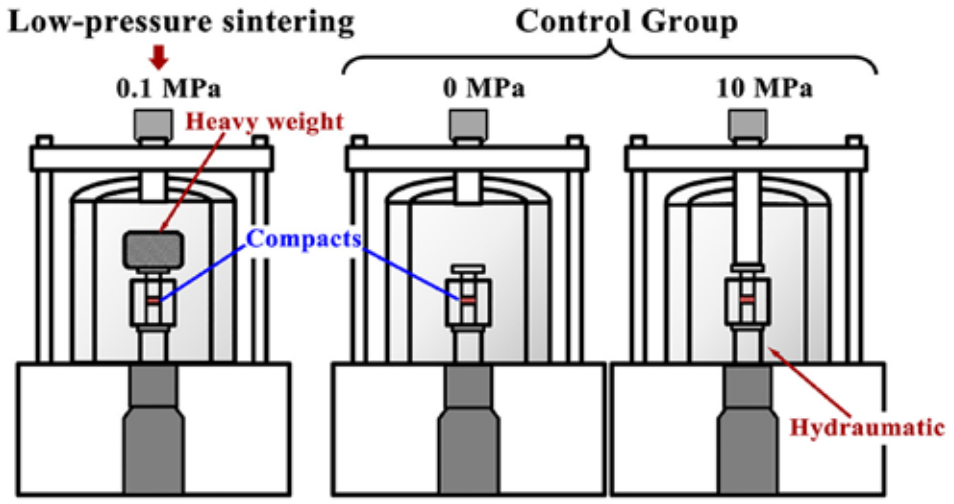

Figure 2: Schematic presentation of low-pressure sintering and its control group in this research.

2.2 Experimental techniques

Fixed mass 2024Al pre-alloyed powders were compacted into a disc (40 mm diameter × 2.07 mm thickness) under an axial pressure of 400 MPa. After compacts were inserted into a high-strength graphite mold, the sintering experiments were carried out in a precision vacuum hot-pressing furnace (VVP-60). The sintering pressure was set to three different orders of magnitude: 0 MPa, 0.1 MPa, and 10 MPa, as demonstrated in Figure 2. Of these, the pressure of 0.1 MPa was achieved using a 15 kg iron weight, and the pressure of 10 MPa relied on hydraulic pressure from the hydraulic station. The sintering temperatures were set to 525°C and 575°C, near solidus and above respectively, which represented two kinds of sintering features: almost no liquid phase formation and a small amount. After reaching the set temperature with a heating rate of 10°C/min, specimens were isothermally held for 2 hours, followed by cooling to 200°C at 5°C/min and then furnace cooling. Considering chemical activities of aluminum, the furnace was evacuated to a vacuum of 10^{-3}Pa.

The density of specimens under different sintering conditions was measured using the Archimedes drainage method with an MSA324S-000-DU balance. The thickness of compacts before and after sintering was respectively measured with a vernier caliper. To observe the microstructure of sintered aluminum, the middle part of the specimens was cut by wire-electrode cutting and embedded in the urea formaldehyde resin. The cross-section of sintered aluminum was grinded with emery-paper and polished with 0.05 μm alumina suspensions. Scanning electron micrographs were captured in backscatter mode using a scanning electron microscope (SEM; model: Quanta 250 FEG, FEI). Surface distribution of main elements such as Al, Cu, and Mg in 2024Al were evaluated by an electron probe micro-analyzer (model: JXA-8530 F). Phase identification was conducted by X-ray diffraction in the range of 20° to 90° at a scan rate of 5°/min with a Bruker Advance D8. High magnification details in sintered aluminum were investigated via a Transmission Electron Microscope (TEM; Tecnai G2 F20). An electronic universal testing machine (Instron 3369) was employed to carry out tensile tests, and the fracture modes were characterized by scanning electron micrographs.

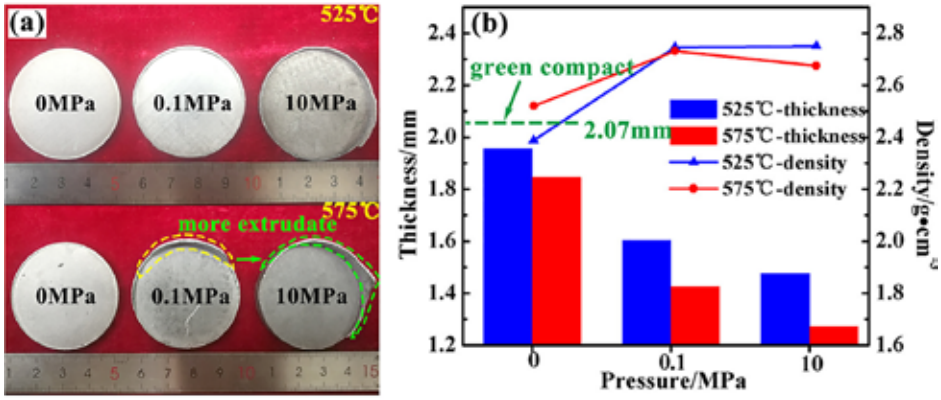

Figure 3: (a) Photograph of sintered compacts at different conditions, (b) the thickness and density of sintered compacts at different conditions.

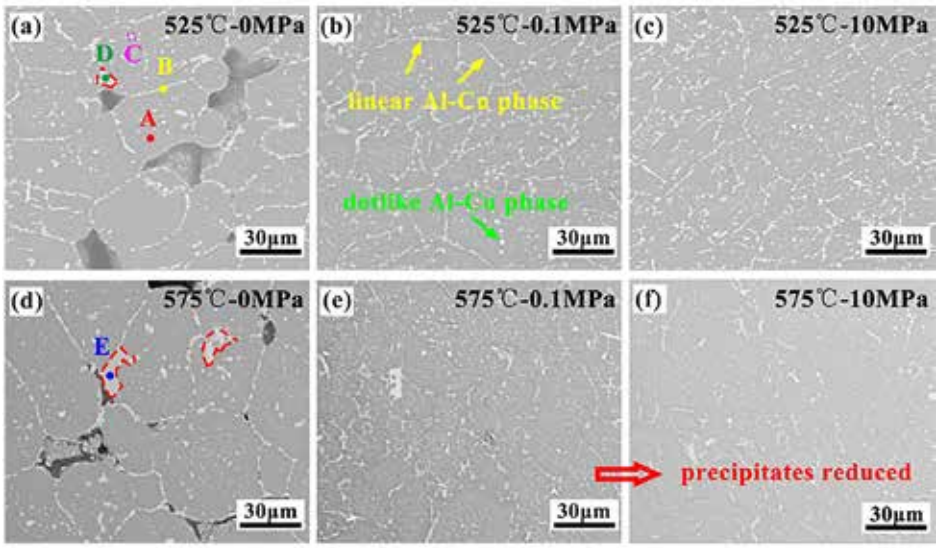

Figure 4: SEM micrographs of sintered aluminum under different pressure states at 525°C and 575°C: (a) 525°C, 0 MPa; (b) 525°C, 0.1 MPa; (c) 525°C, 10 MPa; (d) 575°C, 0 MPa; (e) 575°C, 0.1 MPa; (f) 575°C, 10 MPa.

Position	Al	Cu	Mg	Fe	Mn	Si
A	96.52	1.48	2.00	–	–	–
B	71.61	26.23	1.77	–	–	0.39
C	81.87	14.36	3.21	0.56	–	–
D	79.75	13.80	1.60	4.11	0.74	–
E	72.18	2.01	–	6.30	19.51	–

Table 2: Chemical composition of the characteristic position in Figure 4 (wt%).

3 RESULTS AND DISCUSSION

3.1 Compacts deformation and density

The photograph of compacts sintered at different conditions is shown in Figure 2a. The specimens prepared via pressureless sintering at 525°C and 575°C basically maintained the initial disk morphology of the green compact. As loading pressure, the edge of sintered compacts was extruded out along the fit clearance of the graphite mold in different degrees, especially at 575°C. As indicated by the dashed line in Figure 2a, the edge extrudate of the compact sintered under 0.1 MPa at 575°C is apparently less than that under 10 MPa.

Figure 3b presents the thickness and density of sintered aluminum under different pressure states at 525°C and 575°C. Compared to the thickness of a green compact (2.07 mm), the shrinkage caused via pressureless sintering was very limited. The density of the pressureless sintered aluminum was also much lower than that of the same grade as cast aluminum alloy (2.76 g/cm^3) [11]. Apparently, it is difficult for pre-alloyed aluminum powder to realize densification via pressureless sintering.

After loading pressure, the shrinkage of compacts was obvious, even if the pressure was only 0.1 MPa. The density of aluminum sintered under 0.1 MPa at 525°C rapidly increased to 2.747 g/cm^3, which indicated pre-alloyed aluminum powders could reach densification via low pressure. While further increasing the loading pressure to 10 MPa at 525°C, the gain for density (from 2.747 g/cm^3 to 2.751 g/cm^3) was not apparent. Another noteworthy phenomenon was the density did not always trend positive with the shrinkage on dimensions with the sintering temperature rising to 575°C, even decreased slightly (2.732 g/cm^3 of 0.1 MPa and 2.675 g/cm^3 of 10 MPa). This phenomenon will be discussed in the following section.

3.2 Microstructure and composition analysis

The microstructures of specimens sintered under different pressure states are presented in Figure 4. The gray matrix is aluminum (α-Al), and the white phases are precipitates formed during sintering. The EDS spectral results of each marked position (A-E) in Figure 4a and d are listed in Table 2, including all kinds of feature regions in sintered aluminum. From point A, the gray aluminum base contains a small amount of Cu and Mg, while the white precipitates are rich in alloying elements such as Cu and Mg (Point B and C). Some coarse blocky precipitates distributed at the triangular position marked by red dashed lines in Figure 4a and d contained more impurity elements such as Fe and Mn than other regions (Point D and Point E). These precipitates are insoluble for the aluminum matrix and have a lower melting point to form liquid during heat treatment in the review paper by Wang and Starink [12]. In the following discussion, these white precipitates are collectively called Al–Cu phases. The morphologies of white Al–Cu phases mainly included linear distribution at the particle/grain boundary and dot-like dispersion inside the powder, as indicated in Figure 3b.

With the change of sintering temperature and pressure, the microstructure of the corresponding aluminum alloys exhibited different characteristics. Figure 4a and 4d show the microstructure of specimens underwent pressureless sintering at 525°C and 575°C respectively, and there were still some pores left in the compacts. These residual pores were neither closed via sintering shrinkage nor filled by liquid formed via eutectic reaction (Figure 4d). That is to say, it is difficult for pre-alloyed aluminum powders to achieve densification by pressureless sintering.

Compared with pressureless sintering, the microstructure of sintered aluminum apparently varied with loading pressure. Under a low pressure of 0.1 MPa at 525°C, residual pores in the compact were closed by the rearrangement and the plastic deformation of aluminum powders (Figure 4b). Every particle was closely combined with each other. Base on this fact, it can be concluded that low-pressure sintering could make pre-alloyed aluminum powders realize high

densification. The microstructure of the sintered aluminum under 10 MPa at 525°C was similar to that of 0.1 MPa (Figure 4c). When the temperature rose to 575°C, the decrease in plasticity and the formation of liquid led to more thorough deformation for aluminum powders under the same pressure. Compared with the specimens sintered at 525°C, there was a slight decrease of the linear precipitates at the powder boundary, which were replaced by the coarse blocky precipitates formed at the triangular particle boundary, as seen in Figure 4e. This was related to particle deformation caused by low pressure. The liquid converged to the triangular boundary due to pressing and solidified into coarse precipitates. When the loading pressure further increased to 10 MPa, the most obvious change in sintered aluminum was the content of white precipitates comparatively decreased than that of 0.1 MPa, as indicated by Figure 4f. Combined with the phenomenon of slightly decreased density mentioned earlier, there may be a correlation between both.

In order to clarify this correlation, the area distribution characteristic of element concentration of the edge extrudate formed under 10 MPa at 575°C was analyzed by EPMA technology, and the results are shown in Figure 5. It can be seen that the edge extrudate presented a typical eutectic solidification feature (Figure 5b), which contained a large amount of Cu (Figure 5d) and Mg (Figure 5e). The result illustrated that the Al–Cu eutectic liquid of aluminum alloy formed during supersolidus sintering was easily squeezed out to the edge of compacts by the loading pressure, and this resulted in the loss of alloy elements such as Cu, Mg, and Fe for aluminum alloy. This was the reason why the density of the aluminum sintered at 575°C decreased slightly, that is, some of the "high weight" elements such as Cu, Fe, and Mn were squeezed out with molten liquid.

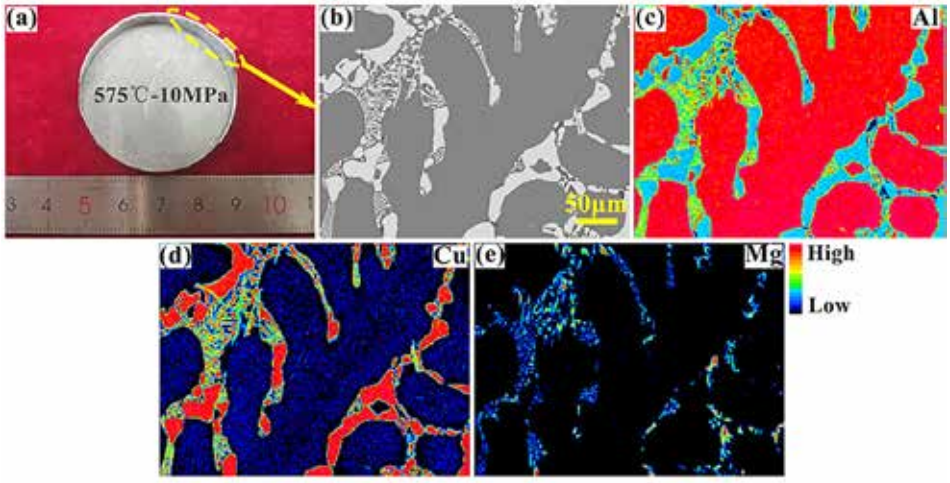

Figure 5: Element maps of the edge extrudate analyzed by EPMA. (a) The compact sintered under 10 MPa at 575°C, (b) SEM micrograph of the edge extrudate, (c) Al map, (d) Cu map, (e) Mg map.

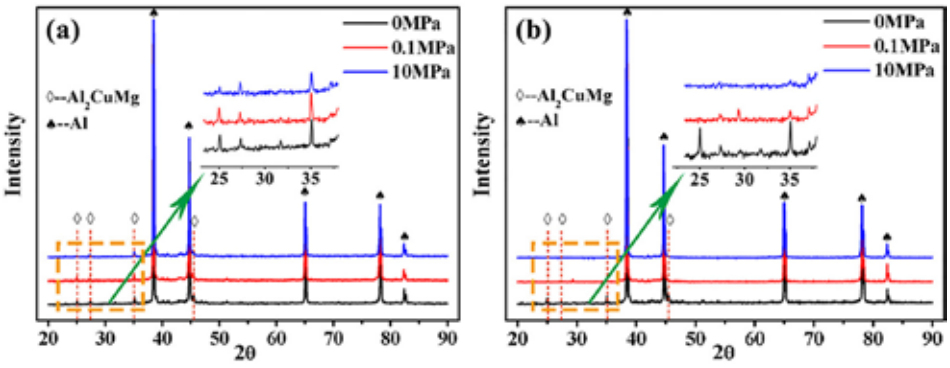

Figure 6: XRD diffraction spectra of aluminum alloys sintered under 0 MPa, 0.1 MPa, and 10 MPa at different temperature: (a) 525°C, (b) 575°C.

Figure 6 shows XRD results of aluminum powders sintered under different conditions. Although there were several combinations of sintering temperature and pressure, the second phase detected in the specimens was only Al_2CuMg (S phase). The phenomenon of precipitates reduced with loading pressure at 575°C was further verified by the XRD results (Figure 6b). The intensity of diffraction peaks corresponding to the Al_2CuMg phase decreased with an increase in pressure, and the peaks almost disappeared when the pressure reached 10 MPa.

Obviously, the pressure is a sensitive factor for aluminum powders sintering at the supersolidus temperature. The formation of the liquid phase led the sintering process to become more complicated. According to the phase diagram, the formation of the liquid phase is mainly because of eutectic reactions. One is the ternary eutectic reaction when the temperature exceeds 507°C:

$$L \rightleftharpoons \alpha(Al) + \theta(CuAl_2) + S(Al_2CuMg) \quad \text{Equation 1}$$

Another is the binary eutectic reaction when the temperature exceeds 550°C:

$$L \rightleftharpoons \alpha(Al) + \theta(CuAl_2) \quad \text{Equation 2}$$

Mi and Grant [13] considered the functional relationship of the liquid phase fraction with temperature during sintering is

$$f_l = \left(\frac{T - T_s}{T_l - T_s}\right)^{(1/(1-k))} \quad \text{Equation 3}$$

f_l is the liquid fraction; T_l is the liquidus temperature; T_s is the solidus temperature, and k is a partition coefficient. Wang et al. [10] demonstrated k was 0.66 in hot isostatic pressing of 2A12 aluminum alloy, which has the same chemical composition as 2024 aluminum alloy. The curve obtained according to this functional relationship between sintering temperature and the fraction of the liquid phase is shown in Figure 7. When the sintering temperature was 525°C, there was only less than 1% liquid in the sintered aluminum; while the temperature rose to 575°C, the liquid fraction rapidly reached 11.47%. The liquid phase distributed at the grain boundaries and prior particle boundaries will cause a rapid-softening, even collapse for aluminum powders, as reported by Momeni et al. [14]. Despite this, as mentioned earlier, pressureless sintering was unable to achieve densification for pre-alloyed powders with liquid phase produced at 575°C. But the yield strength reduction of aluminum powders caused by the temperature rising and liquid phase easily resulted in high densification via low pressure. The Al–Cu phases such as Al_2Cu (θ phase) and Al_2CuMg (S phase) are still the main strengthening phases for heat-treatment strengthening of 2024 aluminum alloy [15,16], and the loss of alloy elements Cu and Mg will weaken the strengthening for sintered compacts. Apparently, this adverse effect in low-pressure sintering was relatively less than that of 10 MPa. That

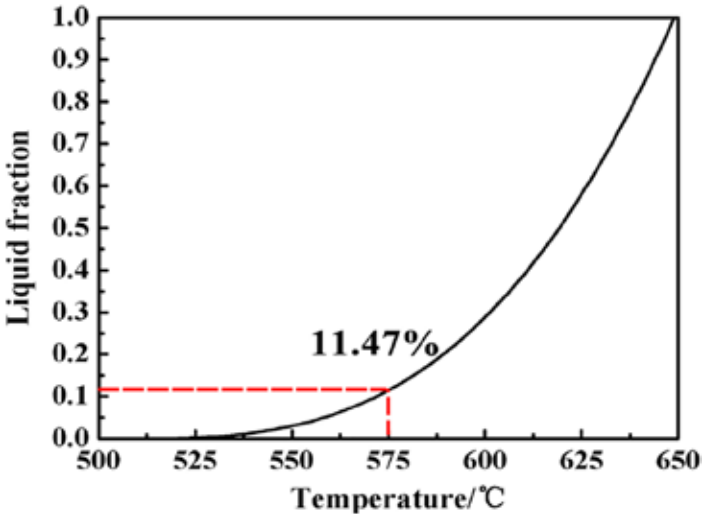

Figure 7: Relationship between liquid phase quantity of 2024 aluminum and temperature.

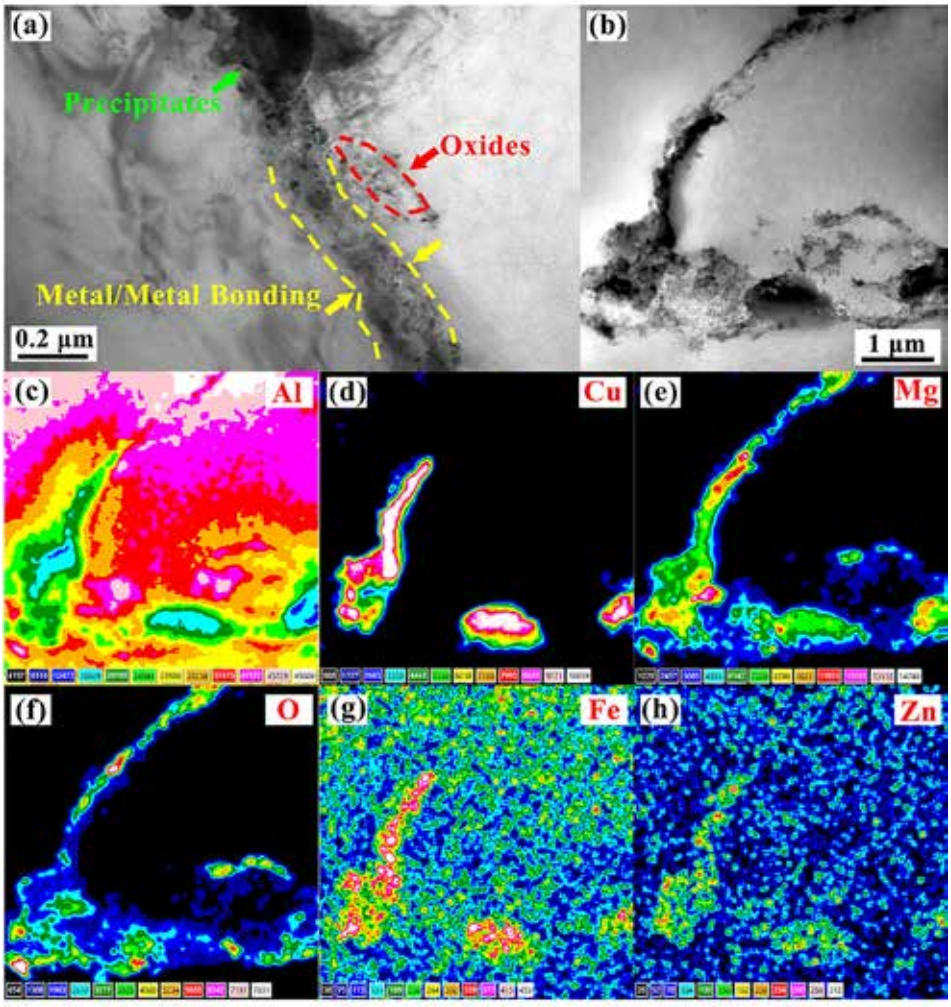

Figure 8: TEM analysis of prior particle boundary of the aluminum sintered under 0.1 MPa at 575°C: (a) and (b) are bright field images of two types of PPB; EDS-acquired elemental maps of (c) Al, (d) Cu, (e) Mg, (f) O, (g) Fe, (h) Zn in (b).

is to say, the low-pressure sintering is more suitable for pre-alloyed aluminum powders at supersolidus temperature.

To gain further insight on microstructure characteristics of low-pressure sintered aluminum, the specimen obtained under 0.1 MPa at 575°C was investigated at higher resolution using TEM. Figure 8 presents the prior particle boundary (PPB) of low-pressure sintering aluminum that can be directly used as an important reference to evaluate the quality of APM. According to the difference in morphology, it is easy to identify the PPB is an irregular transition zone with width less than 0.2 μm between two particles (Figure 8a). The main part of it is the directly metal/metal bonding formed through particles contacting, annotated by a yellow dash line, which is one of the two typical bonding interfaces in the sintered aluminum while the other is a metal/oxide layer/metal bonding interface [17]. Apparently, the effect of this metal/metal bonding on improving the mechanical properties for APM is more critical. From Figure 8a, there were still some Al–Cu precipitates at the boundary and small clusters of oxides crushed by compression distributed in the right particle. The whole boundary reflected a good conjunction between aluminum particles.

Comparing with Figure 8a, Figure 8b shows another more complicated prior particle boundary formed at the triangular junction of aluminum powders with the maximum width close to 1 μm. To further clarify the chemical composition of the boundary in Figure 8b, elemental maps of Al, Cu, Mg, O, Fe, and Zn were obtained by EDS map scanning and presented in Figure 8c–h respectively. It can be seen this coarse transition zone apparently had a complex composition of oxides and precipitates. However, no micro-voids and cracks were observed in this irregular region, which indicated a fully dense transition zone at the triangular particle boundary could be established via low-pressure sintering at 575°C. Besides, the black linear precipitation in Figure 8b, which was rich in alloying element Cu, Mg, Fe, and Zn, was consistent with the feature of liquid solidification and it just reflected the characteristic of low-pressure sintering for pre-alloyed aluminum powders at the supersolidus temperature, that is, a substantial part of liquid phase remained in the sintered structure instead of squeezing out.

Another notable phenomenon is the continuous distribution of heterogeneous oxygen along the PPB and the enrichment of magnesium with the similar distribution of oxygen. As mentioned earlier, the difficulty of APM is always that the stubborn oxide layer on the surface of powders is hard to remove. Many studies have shown adding a small amount of magnesium is an effective means to improve the sinterability of aluminum powders. Coincidence is the 2024Al atomized powders used in this research just contained 1.51wt% Mg (Table 1). That is to say, Mg atoms dissolved in the aluminum transferred to the edge of the powder with the temperature reaching 573°K [18] and would react with the prior aluminum oxide layer above 773°K as follows [19]:

$$3Mg + 4Al_2O_3 \rightarrow 3MgAl_2O_4 + 2Al$$

Equation 4

When the Mg concentration in the region is high enough (4%–8%), reaction 2 tends to occur.

$$3Mg + Al_2O_3 \rightarrow 3MgO + 2Al$$

Equation 5

Xie et al. [20] study shows when the mass fraction of Mg is in the range of 1.0–2.0 %, two reduction products, $MgAl_2O_4$ and MgO, tend to form. The fresh Al atoms produced by the deoxidization reaction and the shear stress caused by the phase volume change with the new formation of $MgAl_2O_4$, MgO led to the destruction of the aluminum oxide film and the formation of a new metallic bond between particles. However, compared with pressureless sintering mentioned earlier, it can be inferred the densification of pre-alloyed aluminum powders could not be achieved only depending on the reaction of Mg atoms. Therefore, the key to achieve metallurgical bonding between aluminum powders still relied on the direct compression of powders caused by low pressure.

Figure 9 exhibits some crystal characteristics inside the powder after low-pressure sintering. Plenty of dislocations remained in the aluminum after sintering and formed dislocation tangles as the movement hindered by rod-like precipitates (Figure 9a). Figure 9b shows a grain boundary and Al–Cu phase precipitated along it, which was apparently different from the morphology feature of PPB analyzed before. It indicated aluminum powder was still composed of several grains after sintering, and the precipitated phases in the powder were evenly dispersed in the grain and at the grain boundary. Due to the furnace cooling mode of aluminum alloy after sintering, the precipitates inside the powder are mainly rod-shaped and finer needle-shaped, as seen in Figure 9c. According to the EDS map scanning for Figure 9c, the precipitates in the crystal mainly were Al_2CuMg (S phase) and Al–Cu phase enriched with Mn and Fe. In addition, there is no obvious oxidation inside the powder (Figure 9h), compared with PPB. Obviously, the aluminum alloy sintered under low pressure had unique crystal structure characteristics different from that of cast aluminum alloy and determined the unique mechanical properties of aluminum powder metallurgy alloy.

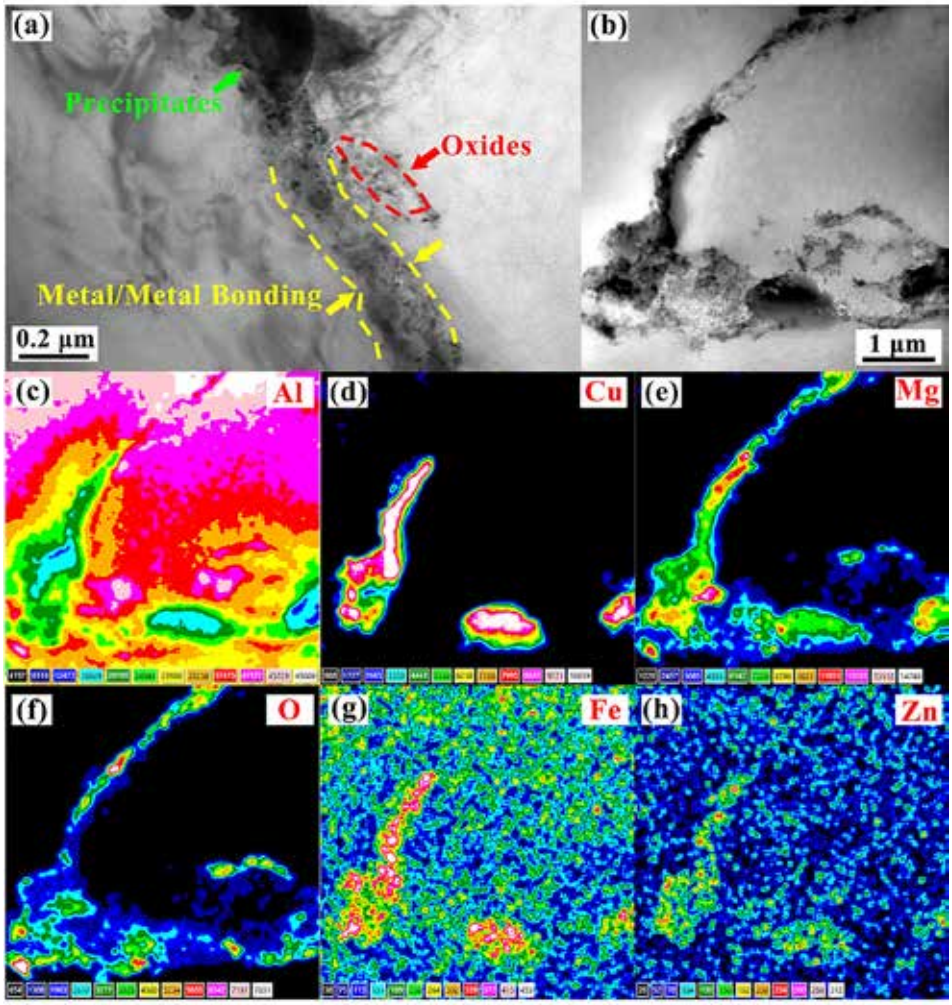

Figure 9: TEM analysis inside powder of the aluminum sintered under 0.1 MPa at 575°C: (a) dislocation, (b) grain boundary, (c) precipitates are bright field images respectively; EDS-acquired elemental maps of (d) Cu, (e) Mg (f) Mn, (g) Fe, (h) O in (c).

3.3 Tensile properties and fracture characteristics

Figure 10 shows the tensile properties of aluminum prepared under different sintering conditions and the comparison with other literatures. Figure 10a and c present the average ultimate tensile strength (UTS) at 525°C and 575°C respectively. It can be seen that the UTS of pressureless sintering aluminum was far inferior to that of pressure sintering at the same temperature, while the UTS of the aluminum alloy sintered under 0.1 MPa at 525°C was 153.46 MPa and further reached 226.18 MPa with the temperature rising to 575°C, which was already superior to that of cast 2024-T1 aluminum alloy as specified in ASTM B595. For higher loading pressure (10 MPa), the tensile strength of sintered aluminum was always higher than that of low-pressure sintering. But the UTS gap between 226.18 MPa and 233.64 MPa was close at 575°C. For powder metallurgy aluminum with powder as a structural unit, the mechanical property mainly depended on the bonding state between powders. The loading pressure not only increased the relative density of the sintered aluminum,

It was difficult to achieve densification of pre-alloyed aluminum powders prepared via pressureless sintering. However, low-pressure sintering was suitable.

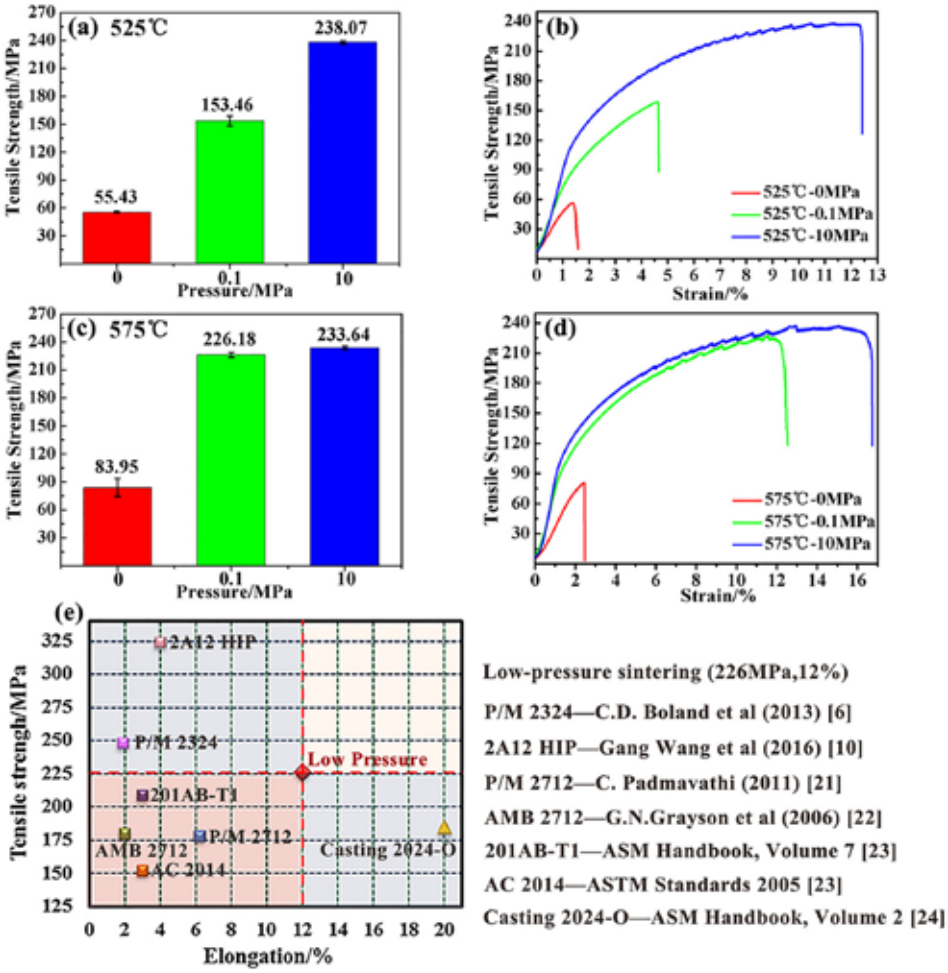

Figure 10: Tensile properties of aluminum alloys sintered under different pressure states: (a) the UTS at 525°C; (b) the stress–strain curves at 525°C; (c) the UTS at 575°C; (d) the stress–strain curves at 525°C; (e) Comparison with other literatures.

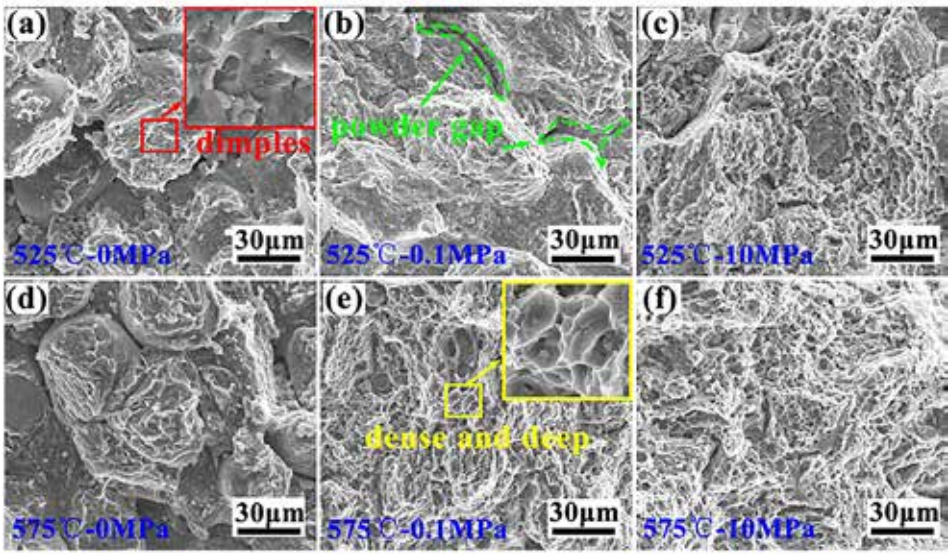

Figure 11: Fracture morphology of aluminum alloys sintered under different conditions: (a) 525°C, 0 MPa; (b) 525°C, 0.1 MPa; (c) 525°C, 10 MPa; (d) 575°C, 0 MPa; (e) 575°C, 0.1 MPa; (f) 575°C, 10 MPa.

but it also destroyed the initial oxide layer on the surface of the particles, which promoted the metallurgical bonding between the aluminum powders. Apparently, the higher the pressure meant the better tensile properties.

According to the stress–strain curves of all the specimens (Figure 10b and d), the plasticity of sintered aluminum also exhibited the similar rule of the tensile strength. Among them, the elongation of the aluminum sintered under 0.1 MPa at 575°C was almost 12%. A comparison of low-pressure sintering 2024 aluminum with other literatures is exhibited in Figure 10e [6, 10, 21, 22, 23, 24]. Apparently, the ductility of low-pressure sintering aluminum is superior to other similar aluminum PM alloys, and the tensile strength is also higher than that of casting 2024 aluminum at the O state, which means the low-pressure sintering helps APM achieve a good balance between ductility and strength.

Combined with tensile properties mentioned earlier for low-pressure sintering of pre-alloyed aluminum powders, the key to obtaining good mechanical properties is a suitable sintering temperature. In this study, the suitable temperature was 575°C, which caused a significant decrease to yield strength of the powders and generated a small amount of liquid. Therefore, the low pressure is sufficient to close the residual pores and make the particles fully contact to destroy the oxide layer during sintering. In addition, according to the similar tensile properties of the aluminum sintered under 10 MPa at 525°C and 575°C respectively (238.07 MPa and 233.64 MPa), it can be assumed the mechanical properties of sintered aluminum will reach an extreme value if the bonding at the prior particle boundary is sufficient.

Figure 11 shows the fracture morphology of aluminum alloys that were sintered under different conditions. The fracture morphology of the pressureless sintered aluminum shows powders were not fully in contact with each other (Figure 11a and d), and the fracture left dimples at the powder connect surface, as indicated by a local magnification in Figure 11a. This indicated the failure mode was peeling along the powder boundary for pressureless sintered aluminum. After loading pressure, the plastic deformation of Al powders caused the compact to be tight over the entire surface. The fracture morphology of the specimen sintered under 0.1 MPa at 525°C was mainly composed of shallow dimples and tearing ridges (Figure 11b), which indicated the failure mode was mainly a quasi-dissociation fracture. Also, there were some powder gaps left at the fracture surface, as indicated by the green dashed line, which means the powder bonding was not strong enough under 0.1 MPa at a low temperature (525°C). With an increase in temperature, the consolidation between powders was firm and dimples at the fracture surface were distinctly more dense and deeper than that of 525°C, as seen by a local magnification in Figure 11e. The fracture mode of the low-pressure sintering

aluminum obtained at 575°C was a typical plastic fracture, which consisted of compacts sintered under 10 MPa (Figure 11c and f).

4 CONCLUSIONS

From the above study on the microstructures and tensile properties of aluminum alloys that were sintered under different pressure states, the main conclusions are as follows:

›› It was difficult to achieve densification of pre-alloyed aluminum powders prepared via pressureless sintering. However, low-pressure sintering was suitable.

›› Due to squeezing out of liquids at supersolidus temperature, the loss of alloying elements such as Cu and Mg via low-pressure sintering was relatively less than that of 10 MPa, which was more beneficial for subsequent heat treatment.

›› Although the structure and composition of the prior particle boundary were quite complicated, including precipitates and oxides, there were no micro-voids and cracks at the boundary, which indicated a good metallurgical bonding between aluminum powders formed via low-pressure sintering.

›› A suitable temperature condition was the key for low-pressure sintered aluminum to obtain a good mechanical performance. The 2024Al powders sintered under a low pressure of 0.1 MPa at 575°C had a density of 2.732 g/cm^3 and a ultimate tensile strength of 228.16 MPa with ductility of 12%, which achieved a good balance of ductility and strength.

DECLARATION OF COMPETING INTEREST

The authors declare that they have no known competing financial interests or personal relationships that could have appeared to influence the work reported in this paper.

ACKNOWLEDGMENTS

The research reported in this paper was financially supported by the National Basic Research Program of China (No. 61xxxx02). The authors thank Prof. Ma and Prof. Liu for the instructive suggestions and valuable comments on the writing of this article.

REFERENCES

[1] Von Hehl A, Krug P. Aluminum and aluminum alloys. Struct. Mater. Process. Transp.. Weinheim, Germany: Wiley-VCH Verlag GmbH & Co. KGaA; 2013. p. 49e112. https://doi.org/10.1002/9783527649846.ch2.

[2] Rahimian M, Ehsani N, Parvin N, H reza Baharvandi. The effect of particle size, sintering temperature and sintering time on the properties of Al-Al2O3 composites, made by powder metallurgy. J Mater Process Technol 2009;209:5387e93. https://doi.org/10.1016/j.jmatprotec.2009.04.007.

[3] Sun C, Song M, Wang Z, He Y. Effect of particle size on the microstructures and mechanical properties of SiC-reinforced pure aluminum composites. J Mater Eng Perform 2011;20:1606e12. https://doi.org/10.1007/s11665-010-9801-3.

[4] Kwon H, Mondal J, AloGab K, Sammelselg V, Takamichi M, Kawaski A, et al. Graphene oxide-reinforced aluminum alloy matrix composite materials fabricated by powder metallurgy. J Alloys Compd 2017;698:807e13. https://doi.org/10.1016/j.jallcom.2016.12.179.

[5] Qian M, Schaffer GB. Sintering of aluminium and its alloys. Woodhead Publishing Limited. 2010. https://doi.org/10.1533/9781845699949.3.291.

[6] Boland CD, Hexemer RL, Donaldson IW, Bishop DP. Industrial processing of a novel Al-Cu-Mg powder metallurgy alloy. Mater Sci Eng, A 2013;559:902e8. https://doi.org/10.1016/j.msea.2012.09.049.

[7] Sweet GAW, Amirkhiz BS, Williams BW, Taylor A, Hexemer RL, Donaldson IW, et al. Microstructural evolution of a forged 2XXX series aluminum powder metallurgy alloy. Mater Char 2019;151:342e50. https://doi.org/10.1016/j.matchar.2019.03.033.

[8] Cooke RW, Kraus NP, Bishop DP. Spark plasma sintering of aluminum powders pre-alloyed with scandium additions. Mater Sci Eng, A 2016;657:71e81. https://doi.org/10.1016/j.msea.2016.01.053.

[9] Khalil A, Hakeem AS, Saheb N. Optimization of process parameters in spark plasma sintering Al6061 and Al2124 aluminum alloys. Adv Mater Res 2011;328e330:1517e22. https://doi.org/10.4028/www.scientific.net/AMR.328-330.1517.

[10] Wang G, Lang LH, Yu WJ, Huang XN, Li F. Influences of hot isostatic-pressing temperature on the microstructure, tensile properties and tensile fracture mode of 2A12 powder compact. Acta Metall Sin (English Lett 2016;29:963e74. https://doi.org/10.1007/s40195-016-0482-2.

[11] Association A. Aluminum standards and date. The aluminum association,inc. 2000.

[12] Wang SC, Starink MJ. Precipitates and intermetallic phases in precipitation hardening Al-Cu-Mg-(Li) based alloys. Int Mater Rev 2005;50:193e215. https://doi.org/10.1179/174328005X14357.

[13] Mi J, Grant PS. Modelling the shape and thermal dynamics of Ni superalloy rings during spray forming. Part 2: thermal modelling - heat flow and solidification. Acta Mater 2008;56:1597e608. https://doi.org/10.1016/j.actamat.2007.12.022.

[14] Momeni H, Shabestari SG, Razavi H. Rheology of Al-Cu-Mg pre-alloyed powder in supersolidus liquid phase sintering process. Can Metall Q 2017;56:442e9. https://doi.org/10.1080/00084433.2017.1361181.

[15] Kent D, Schaffer GB, Drennan J. Age hardening of a sintered Al-Cu-Mg-Si-(Sn) alloy. Mater Sci Eng, A 2005;405:65e73. https://doi.org/10.1016/j.msea.2005.05.104.

[16] Wang SC, Starink MJ, Gao N. Precipitation hardening in Al-Cu-Mg alloys revisited. Scr Mater 2006;54:287e91. https://doi.org/10.1016/j.scriptamat.2005.09.010.

[17] Xie G, Ohashi O, Song M, Furuya K, Noda T. Behavior of oxide film at the interface between particles in sintered Al powders by pulse electric-current sintering. Metall Mater Trans A Phys Metall Mater Sci 2003;34(A):699e703. https://doi.org/10.1007/s11661-003-0104-2.

[18] Kimura A, Shibata M, Kondoh K, Takeda Y, Katayama M, Kanie T, et al. Reduction mechanism of surface oxide in aluminum alloy powders containing magnesium studied by x-ray photoelectron spectroscopy using synchrotron radiation. Appl Phys Lett 1997;70:3615e7. https://doi.org/10.1063/1.119250.

[19] Lumley RN, Sercombe TB, Schaffer GB. Surface oxide and the role of magnesium during the sintering of aluminum. Metall Mater Trans A Phys Metall Mater Sci 1999;30:457e63. https://doi.org/10.1007/s11661-999-0335-y.

[20] Xie G, Ohashi O, Sato T, Yamaguchi N, Song M, Mitsuishi K, et al. Effect of Mg on the sintering of Al-Mg alloy powders by pulse electric-current sintering process. Mater Trans 2004;45:904e9. https://doi.org/10.2320/matertrans.45.904.

[21] Padmavathi C, Upadhyaya A. Sintering behaviour and mechanical properties of Al-Cu-Mg-Si-Sn aluminum alloy. Trans Indian Inst Met 2011;64:345e57. https://doi.org/10.1007/s12666-011-0089-2.

[22] Grayson GN, Schaffer GB, Griffiths JR. Fatigue crack propagation in a sintered 2 xxx series aluminium alloy. Mater Sci Eng, A 2006;434:1e6. https://doi.org/10.1016/j.msea.2006.07.017.

[23] Committee A. Powder metal technologies and applications. ASM International. 1998.

[24] Committee A. Properties and selection: nonferrous alloys and special-purpose materials. Metals Handbook. 1990.

ABOUT THE AUTHORS

Lei Wu, Zhaoji Yu, Chao Liu, Yunzhu Ma, Yufeng Huang, Tao Wang, Lun Yang, Huanyuan Yan, and Wensheng Liu are with the National Key Laboratory of Science and Technology on High-strength Structural Materials, Central South University, Changsha, 410083, China.